中国激光

激光功率对高强 Al-Mg-Si-Cu 合金激光-CMT 复合焊接接头组织性能的影响

张禄中[1,2]，王晓南[2*]，陈夏明[2,3]，陈文刚[1**]，李响[4]，长海博文[3]

[1]西南林业大学机械与交通学院，云南 昆明 650224；

[2]苏州大学沙钢钢铁学院，江苏 苏州 215021；

[3]苏州大学高性能金属结构材料研究院，江苏 苏州 215021；

[4]无锡锐科光纤激光技术有限责任公司，江苏 无锡 214174

摘要 采用激光-CMT 复合焊接工艺(CMT，冷金属过渡)对 2 mm 厚 400 MPa 级 Al-Mg-Si-Cu 合金进行焊接，研究了激光功率对焊接接头宏观形貌及组织性能的影响。研究表明：激光功率达到 3.6 kW 时可获得全熔透焊接接头，随着激光功率的增加，熔宽不断增加而焊缝余高有所降低。熔宽增加和余高降低使得焊缝稀释率增加，焊缝中硅元素含量降低。随着激光功率的增加，焊缝中烧损的镁元素增加，镁元素含量亦有所降低。焊缝中镁和硅元素含量的降低导致固溶强化效果减弱。随着激光功率的增加，全熔透焊缝的硬度逐渐降低。密集气孔的存在进一步恶化了焊缝性能，导致拉伸过程中焊缝处的断裂。焊接接头抗拉强度亦呈不断降低的趋势，在激光功率为 3.6 kW 时，焊接接头的平均硬度和抗拉强度分别达到基材的 65%(85 HV)和 64%(271 MPa)。

关键词 激光技术；高强 Al-Mg-Si-Cu 合金；激光-CMT 复合焊接；显微组织；力学性能

中图分类号 TG457.14 **文献标志码** A **DOI**：10.3788/CJL220681

1 引 言

Al-Mg-Si 合金作为一种可热处理铝合金，具有密度低、力学性能好、成形性好、耐腐蚀性好等优点，在高速铁路、汽车、航空航天等领域得到了广泛应用[1-3]。近几十年来，研究者从微合金化、加工硬化及预拉伸等方面对 Al-Mg-Si 合金的强韧性进行不断提高。其中，在 Al-Mg-Si 合金中添加 Cu 元素更经济、更适用，它不仅提高了峰值时效后的力学性能，而且提高了时效硬化效率[4-5]。研究表明，高强 Al-Mg-Si-Cu 合金在峰值时效时的极限抗拉强度可达 400 MPa，显著高于现有商用 Al-Mg-Si 合金的抗拉强度[6]。

对于可热处理铝合金而言，焊接过程中热影响区中原有的纳米强化相失去作用而发生软化，严重恶化了焊接接头的力学性能[7-8]。为降低热影响区的软化程度，研究者通过焊接技术革新有效降低了热输入，从而改善了热影响区的软化行为。Braun 等[9]利用热输入较低的激光焊接和搅拌摩擦焊，提高了传统冷金属过渡(CMT)焊接工艺的渗透能力并降低了孔隙率，但是焊接接头仍然存在焊缝强度不足的问题。在此基础上，Braun 等[10]为了进一步改善 Al-Mg-Si-Cu 合金焊接接头的力学性能，采用 Al-Si 粉末、Al-Mg 粉末提高了焊缝处的力学性能，但是这种方法无法实现产业化应用。激光-CMT 复合焊接是一种很有前途的高性能、低焊接变形的焊接技术，它利用了激光焊接和 CMT 焊接的优点，克服了单一激光焊接和传统电弧焊接的缺点[11]，两种热源的组合可同时提高生产率和改善焊接质量。研究发现，在激光-电弧复合焊接中，电弧功率控制焊缝宽度而激光功率控制熔深[12]。此外，激光束还可以稳定电弧电压和电流并且能降低柱状电阻，从而提高焊缝的深宽比。而激光-CMT 复合焊接可在降低常规 Al-Mg-Si 合金热影响区软化程度的同时，有效提高焊缝强度，焊接接头抗拉强度可达到基材的 80%[13]。关于激光-CMT 复合热源下高强 Al-Mg-Si-Cu 合金的焊接性研究鲜有报道。

本文以 T6 态高强(400 MPa 级)Al-Mg-Si-Cu 合金为研究对象，研究了激光功率对焊接接头宏观形貌和组织性能的影响，并以此为基础评价了激光-CMT 复合焊接技术应用于高强 Al-Mg-Si-Cu 合金的可能性。

2 试验材料与方法

焊接试验材料采用山东魏桥轻量化材料有限公司

收稿日期：2022-03-21；**修回日期**：2022-04-16；**录用日期**：2022-05-07；**网络首发日期**：2022-05-16

基金项目：国家自然科学基金联合项目(U1864209)、国家自然科学基金(51865053)、江苏省“青蓝工程”计划项目

通信作者：*wxn@suda.edu.cn；**chenwengang999@163.com

生产的T6态400 MPa级高强Al-Mg-Si-Cu合金板材，试验板材尺寸为150 mm×130 mm×2 mm。焊接试验前，采用机械方法去除待焊区域表面的氧化膜，清洗后晾干。使用直径为1.2 mm的商用ER-4047焊丝作为填充材料，具体化学成分和基材的力学性能分别如表1和表2所示。

表1　Al-Mg-Si-Cu合金和焊丝的化学成分(质量分数，%)

Table1　Chemical compositions of Al-Mg-Si-Cu alloy and filler wire (mass fraction, %)

Material	Si	Mg	Fe	Mn	Cr	Cu	Zn	Ti	Al
Al-Mg-Si-Cu alloy	0.80-1.00	0.70-0.90	≤0.15	≤0.65	0.20-0.30	<0.50	<0.05	0.20-0.30	Bal.
Filler wire	12.00	≤0.10	≤0.80	≤0.15	-	≤0.03	≤0.10	-	Bal.

表2　Al-Mg-Si-Cu合金力学性能

Table 2　Mechanical properties of Al-Mg-Si-Cu alloy

Parameter	Yield strength / MPa	Tensile strength / MPa	Elongation /%
Value	390	420	10.0

激光-CMT复合焊接系统包括焊机、光纤激光器和六轴联动机器人。采用激光-CMT复合焊接工艺对板材进行拼焊，拼焊间隙为0，焊板水平放置在带有凹槽的铜板上并固定在焊接装夹平台上。激光束与焊板的夹角为80°，激光光斑直径为0.3 mm，离焦量为0。CMT焊枪中心与焊板垂直距离为13 mm，夹角为60°，光丝间距为3 mm，如图1所示。在焊接过程中，采用高纯氩气作为保护气，保护气流量为30 L/min。

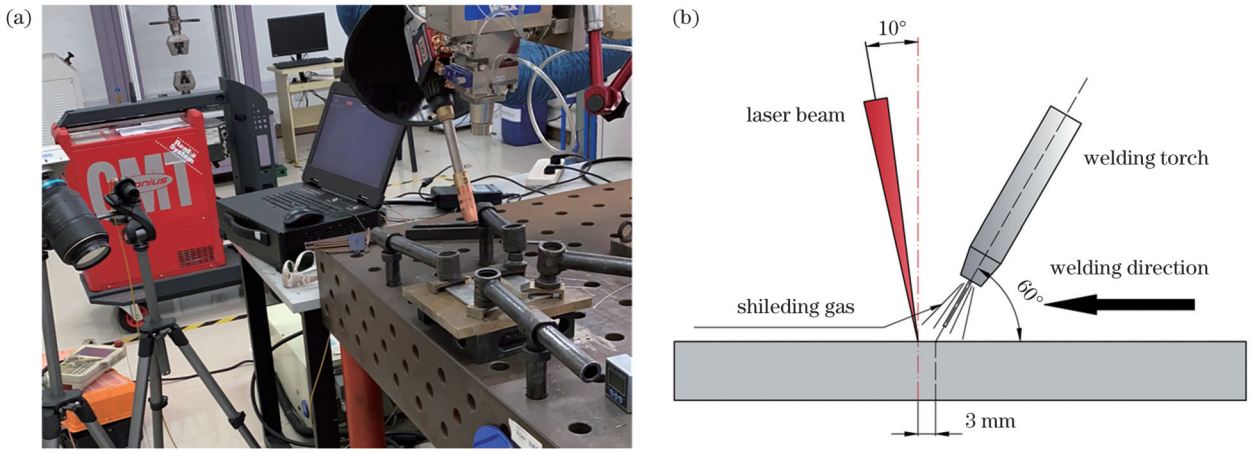

图1　激光-CMT焊接图。(a)试验现场图；(b)焊接示意图

Fig. 1　Laser-CMT welding diagrams. (a) Experimental site map; (b) diagram of welding

本文通过改变激光功率来控制热输入以获得全熔透焊接接头，焊接工艺参数如表3所示。不同激光功率下的焊接热输入为

$$E=\frac{P}{v},\tag{1}$$

式中：E为热输入；P为总功率[12,14]；v为焊接速度。

采用Keller试剂(HF、HCl、HNO_3、H_2O的体积分数分别为1.0%、1.5%、2.5%、95.0%)对精抛后的焊接接头样品进行化学腐蚀，试样腐蚀结束后用乙醇冲洗并冷风吹干。使用金相显微镜和台式扫描电镜(SEM)观察焊接接头宏观形貌和显微组织。采用全自动维氏硬度计测量了焊接接头的显微硬度分布，测试点间隔为0.15 mm，载荷压力为1.96 N，加载时间为10.0 s。采用去除焊缝上、下表面余高的方法消除焊缝余高对接头力学性能的影响，然后对焊接接头进行拉伸性能测试。采用万能试验机进行拉伸试验，拉伸速度为1.0 mm/min，拉伸试样形状如图2所示。

表3　焊接工艺参数

Table 3　Welding process parameters

No.	Laser power /W	Welding speed / (m/min)	Wire feed speed / (m/min)	CMT average current /A	CMT average voltage /V	CMT power /W	Total power /W	Heat input / (J/mm)
S1	3000	4.0	4.0	126	6.0	756.0	3756.0	56
S2	3600	4.0	4.0	119	6.3	749.7	4349.7	65
S3	4200	4.0	4.0	122	6.1	744.2	4944.2	74
S4	4800	4.0	4.0	118	5.9	696.2	5496.2	82

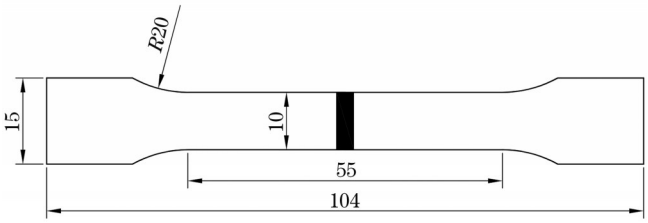

图 2 拉伸试样的尺寸示意图

Fig. 2 Schematic of tensile sample size

3 试验结果

3.1 焊接接头宏观形貌

图 3 给出的是不同激光功率下焊接接头的宏观形貌。可以看出，随着激光功率的增加，焊接接头从未熔透向完全熔透过渡，当激光功率达到 3.6 kW 时获得了全熔透焊接接头。不同激光功率下焊接接头宏观形貌的横截面分区特征明显，分别为热影响区（HAZ）、熔合线（FL）和焊缝（WS）。其中焊缝是由基材金属熔融与焊丝熔化、冷却再结晶后形成的区域；熔合线是接头中焊缝金属向热影响区过渡的区域；热影响区则是焊缝两侧的基材在焊接热循环作用下未熔化，但固态的基材发生明显组织和性能变化的区域[14]。激光功率为 3.0 kW 时，焊接接头出现未熔透现象，如图 3(a)所示。Zhang 等[15]指出，激光功率与电弧之间的协同作用对焊缝形貌有明显影响，且随着激光功率的增加，协同效应逐渐增强。因此，较低的激光功率使得激光与电弧之间的协同作用减弱；由于等离子体的屏蔽作用增强，激光的穿透效率降低。此外，由于铝合金具有较高的热导率，熔池底部未熔透的基材加快了熔池散热，部分基材发生了熔化。在两方面因素的作用下，激光功率为 3.0 kW 时焊接接头中仅有少量基材发生熔化，获得了未熔透焊接接头。而当激光功率增加到 3.6 kW 时，协同作用的增加导致等离子体对激光的屏蔽作用降低，激光穿透效率增加，获得了全熔透焊接接头，如图 3(b)所示。当激光功率进一步增加至 4.2 kW 和 4.8 kW 时，热输入是过量的，大部分能量向焊缝四周扩散，更多的母材发生熔化，焊缝尺寸有所增加，如图 3(c)、(d)所示。

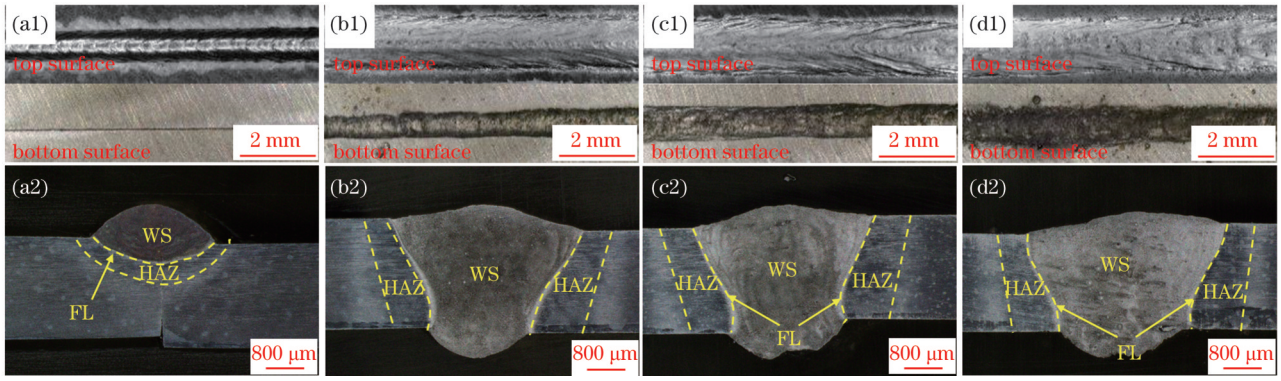

图 3 不同激光功率下的焊接接头宏观形貌。(a1)(a2) 3.0 kW；(b1)(b2) 3.6 kW；(c1)(c2) 4.2 kW；(d1)(d2) 4.8 kW

Fig. 3 Macro morphologies of welded joint under different laser powers. (a1)(a2) 3.0 kW; (b1)(b2) 3.6 kW; (c1)(c2) 4.2 kW; (d1)(d2) 4.8 kW

图 4 给出了焊缝的横截面示意图及焊后接头的熔宽和余高统计结果。由统计结果可知，当激光功率从 3.6 kW 增加到 4.8 kW 时，焊缝的上部熔宽（F_t）从 3.6 mm 增加到 4.0 mm，根部熔宽（F_b）从 2.0 mm 增加到 2.5 mm。当激光功率增加到 4.8 kW 时，热输入达到最大值（82 J/mm），此时焊缝的熔宽最大，如图 4(b)所示。对于全熔透焊接接头，随着激光功率的进一步增加，激光与电弧的协同效应有所减弱[16]，因此熔宽略有增加。而熔宽的增加使得在相同的焊接速度和送丝速度条件下熔池尺寸有所增加，故焊缝余高略有降低。

3.2 焊缝显微组织

图 5 给出了不同激光功率下焊缝中心处的显微组织，其中左下角为观察区域。可以看出，焊缝中心区域均为典型的铸态组织，由大量的等轴晶组成并存在一定数量的微孔。通常显微组织的尺寸取决于热输入[17]，降低热输入会导致冷却速度升高、过冷度增大，从而使得结晶形态以等轴晶为主。然而，Meng 等[16]指出，对于全熔透焊接接头而言，激光与电弧之间的协同效应随激光功率的增加而减弱，热量损失量增加。因此，本文的研究结果表明，激光功率的增加不足以使焊缝中心的等轴晶尺寸发生明显变化。但激光功率的增加势必会导致熔池温度的增加。根据氢溶解度与铝合金熔体温度之间的关系可知，熔池温度的增加使得熔池中的氢溶解度增加，因此在焊缝凝固前更多未来得及逃逸的氢气泡[18]被凝固前沿捕捉，形成细小的氢气孔，如图 5 所示。

图 6 给出了三种焊接接头焊缝边缘的显微组织，左下角为观察区域。可以看出，当激光功率为 3.6 kW 时，FL 附近的柱状晶区平均宽度为 134 μm，如图 6(a)所示。激光功率为 4.2 kW 和 4.8 kW 时，FL 附近的柱状晶区平均宽度分别为 152 μm 和 232 μm，如图 6(b)、(c)所示。一般而言，随着热输入的增加，冷却速度的

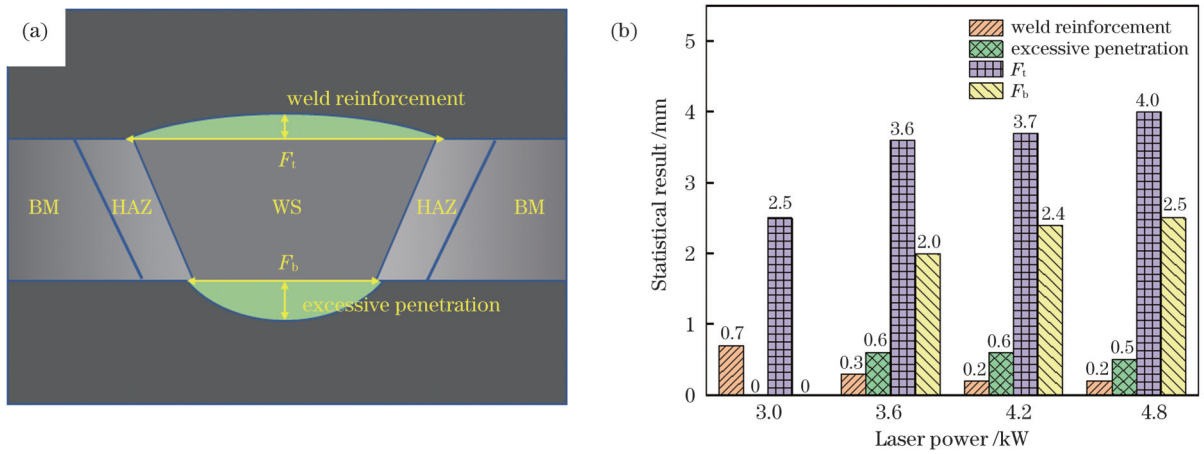

图 4　焊缝横截面示意图及焊缝尺寸统计结果。(a)焊缝横截面示意图;(b)熔宽及余高统计结果

Fig. 4　Schematic of weld cross-section and statistical results of weld sizes. (a) Schematic of weld cross-section; (b) statistical results of melt width and reinforcement

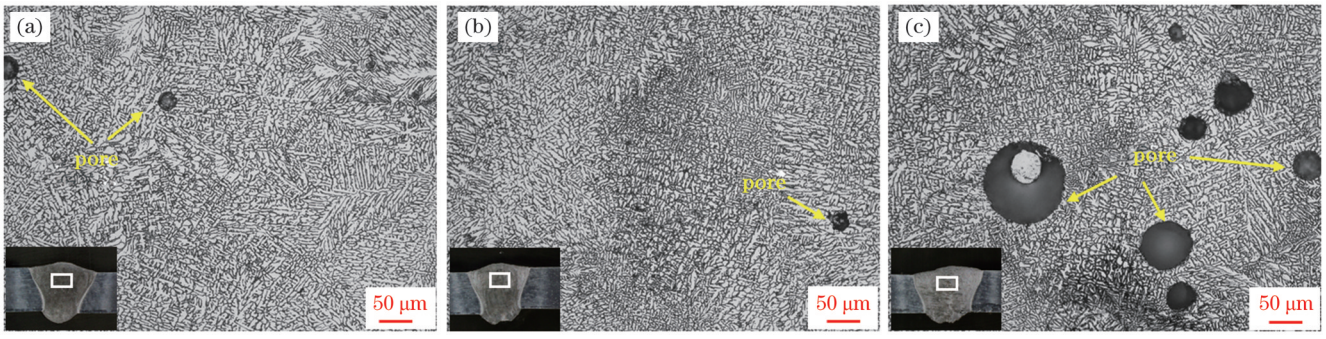

图 5　不同激光功率下的焊缝中心显微组织。(a) 3.6 kW;(b) 4.2 kW;(c) 4.8 kW

Fig. 5　Microstructures of weld center under different laser powers. (a) 3.6 kW; (b) 4.2 kW; (c) 4.8 kW

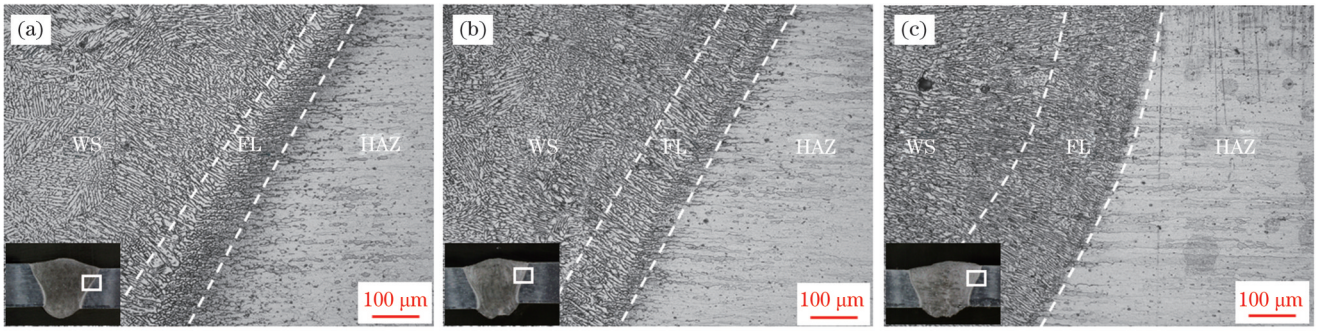

图 6　不同激光功率下的焊缝显微组织。(a) 3.6 kW;(b) 4.2 kW;(c) 4.8 kW

Fig. 6　Microstructures of weld under different laser powers. (a) 3.6 kW; (b) 4.2 kW; (c) 4.8 kW

降低导致过冷度降低,促进了柱状晶的生长[9]。因此,随着激光功率的增加,过冷度的降低抑制了等轴晶的形核,使垂直于熔合线的晶粒向熔池中心择优生长,从而形成较宽的柱状晶区[19-20]。

3.3　焊接接头力学性能

图 7 给出的是全熔透焊接接头横截面的显微硬度分布,左下角为取样区域。可以看出,三种焊接接头的显微硬度分布规律相似,焊缝和热影响区的硬度均明显低于基材(~130 HV)。但不同的是,接头的硬度最低值出现在焊缝处,随着激光功率的增加,焊缝平均硬度和热影响区平均硬度均呈降低趋势。对于高强 Al-Mg-Si-Cu 合金而言,其主要纳米强化相 β″(Mg_5Si_6)[21-24]的热稳定性较差,在焊接热循环的作用下易粗化和转变,使得强化效果减弱,导致热影响区发生明显软化。而激光功率的增加使焊接热输入增加,进一步促进了纳米强化相 β″的粗化和转变,导致热影响区的析出强化效果进一步减弱[25]。因此,随着激光功率的增加,热影响区的软化程度有所增加。但对于焊缝而言,Yan 等[26]指出,由于发生了重熔再结晶,焊缝强度的变化主要依靠固溶强化而非析出强化。焊缝中的固溶强化与焊缝中的元素含量有关。由于焊丝成分、焊接速度及送丝速度相同,三种全熔透焊缝中的各元素含量则与

焊缝稀释率相关。焊缝稀释率(D)的表达式为

$$D=\frac{S_C}{S_A+S_B+S_C},\tag{2}$$

式中:S_A为焊缝上余高横截面面积;S_B为焊缝下余高横截面面积;S_C为焊缝去除上、下余高后的横截面面积。根据式(2)对三种全熔透焊缝的稀释率进行了计算,计算结果如图7(e)所示。结果表明:随着激光功率的增加,焊缝稀释率逐渐升高,焊缝稀释率的升高使焊缝中Si元素含量有所降低。Braun[27]研究发现,焊缝区的硬度随着填充金属中Si含量的增加而增加。而对于采用ER4047焊丝制备的激光-CMT焊缝,Si元素为主要的固溶元素。因此,焊缝中Si元素含量的降低使得焊缝中的固溶强化效果减弱,焊缝硬度有所降低[28]。此外,对于焊缝中另一主要固溶元素Mg元素而言,其作为一种低沸点(1107 ℃)元素,在激光的作用下极易蒸发形成烧损,且随着激光功率的增加,烧损程度增加[29],焊缝中固溶Mg元素含量降低,从而固溶元素带来的固溶强化效果减弱,焊缝的硬度进一步降低。

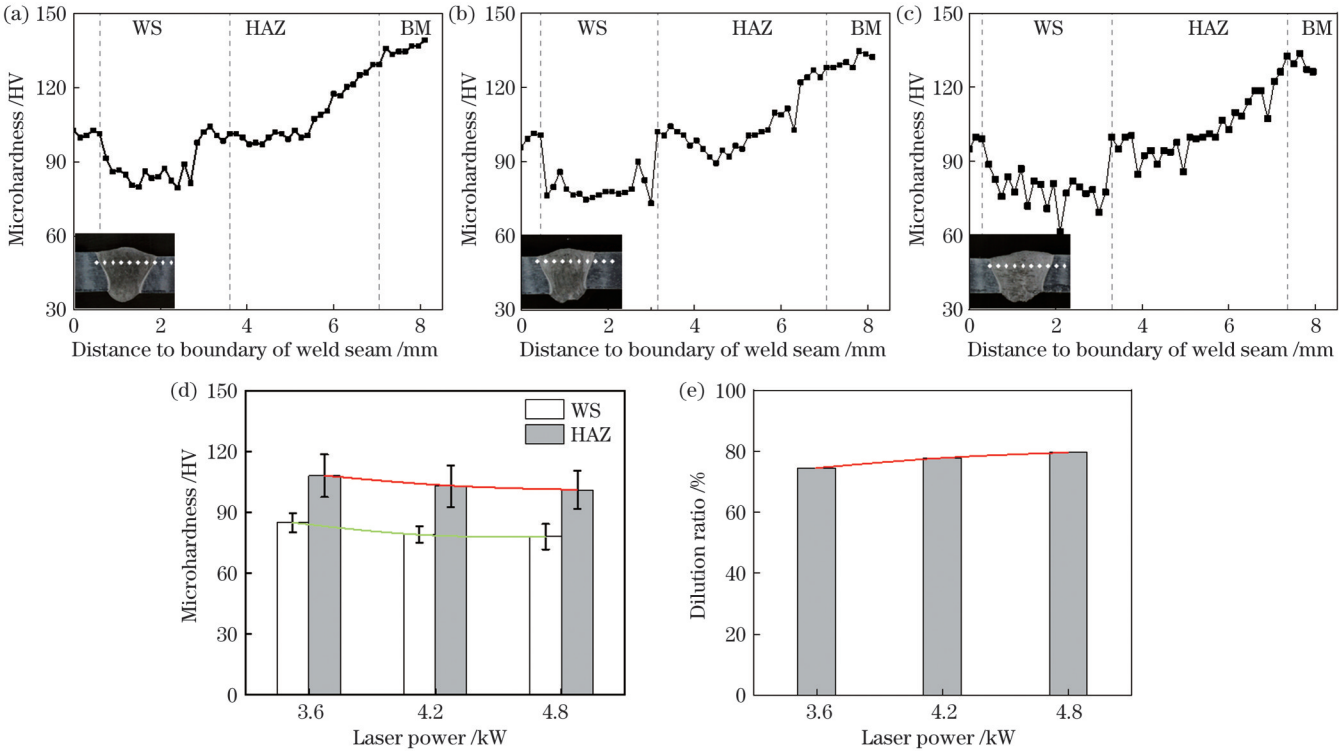

图7　不同激光功率下全熔透焊接接头的显微硬度分布及焊缝稀释率。(a)激光功率为3.6 kW时接头的显微硬度;(b)激光功率为4.2 kW时接头的显微硬度;(c)激光功率为4.8 kW时接头的显微硬度;(d)WS和HAZ的平均显微硬度;(e)稀释率

Fig. 7　Microhardness distributions and weld dilution ratios of full penetration welded joints under different laser powers. (a) Microhardness of joint when laser power is 3.6 kW; (b) microhardness of joint when laser power is 4.2 kW; (c) microhardness of joint when laser power is 4.8 kW; (d) average microhardnesses of WS and HAZ; (e) dilution ratio

图8给出的是不同激光功率下焊接接头拉伸试样的宏观断裂照片及工程应力-应变曲线,接头的拉伸性能如表4所示。可以看出,焊接接头均在焊缝处发生断裂,但激光功率的增加使得焊缝强度有所

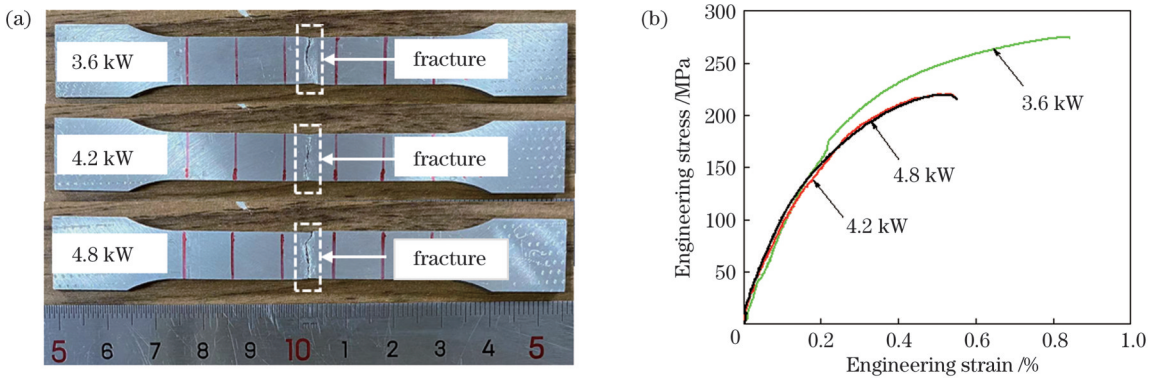

图8　焊接接头拉伸试验结果。(a)接头拉伸断裂位置;(b)拉伸试样的工程应力-应变曲线

Fig. 8　Tensile test results of welded joints. (a) Tensile fracture positions of joints; (b) engineering stress-strain curves of tensile specimens

降低。当激光功率为 3.6 kW 时接头抗拉强度最高(271 MPa),而激光功率为 4.2 kW 和 4.8 kW 时接头抗拉强度分别为 244 MPa 和 220 MPa。由此可见,较低的焊缝硬度使得焊缝成为焊接接头的薄弱位置,而焊缝中密集气孔的存在亦恶化了焊缝的力学性能。因此,焊缝成为焊接接头的薄弱位置,在受力过程中优先发生变形,最终导致焊接接头在焊缝处发生断裂。但整体而言,低激光功率下焊缝软化程度较低且焊接接头的抗拉强度较高,抗拉强度约为基材的 64%。

表 4 焊接接头的拉伸性能

Table 4 Tensile properties of welded joints

Laser power /kW	Tensile strength /MPa	Joint efficiency /%	Elongation /%	Fracture position
3.6	271	64.4	3.0	WS
4.2	244	58.0	1.5	WS
4.8	220	52.2	2.5	WS
Base material	420	100.0	10.0	-

图 9 给出的是不同激光功率下焊接接头在断口处的气孔微观形貌。可以看出,断口内均存在一定数量的细小韧窝和大量直径小于 50 μm 的气孔,未见明显撕裂棱,表现出典型的韧性断裂特征。然而气孔的存在会降低焊缝横截面的有效截面积并产生应力集中,致使焊缝过早发生断裂,这也是焊接接头在焊缝处发生断裂的原因之一。此外,气孔的存在将会显著降低焊接接头的疲劳性能,从而恶化焊接接头的服役寿命[30-32]。因此,为进一步提高高强 Al-Mg-Si-Cu 合金激光-CMT 复合焊接接头焊缝的强度和疲劳性能,降低焊缝气孔率是关键[33]。

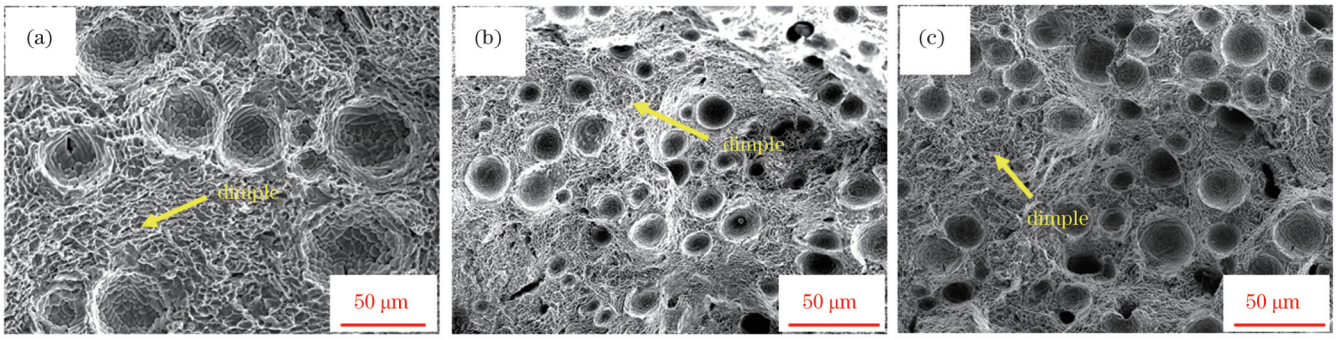

图 9 焊接接头拉伸断口的 SEM 形貌。(a) 3.6 kW;(b) 4.2 kW;(c) 4.8 kW

Fig. 9 SEM morphologies of welded joint tensile fractures. (a) 3.6 kW; (b) 4.2 kW; (c) 4.8 kW

4 结 论

采用激光-CMT 复合焊接工艺对 T6 态高强 Al-Mg-Si-Cu 合金板材进行焊接,研究了激光功率对焊接接头宏观形貌、显微组织及力学性能的影响,主要结论如下:

1) 随着激光功率的增加,焊缝的熔宽呈增大趋势,从 2.5 mm 增加到 4.0 mm。而焊缝余高呈减小趋势,从 0.7 mm 减少至 0.2 mm。当激光功率达到 3.6 kW 及以上时,获得了全熔透焊接接头。

2) 焊缝由柱状晶和等轴晶组成,且随着激光功率的增加,冷却速度和过冷度降低,促进了柱状晶的生长,使得焊缝中的柱状晶区的宽度由 3.6 kW 时的 134 μm 增加至 4.8 kW 时的 232 μm。

3) 激光功率的增加导致焊缝稀释率升高和 Mg 元素烧损程度增加,而焊缝中 Si 和 Mg 元素含量的降低使得焊缝中 Si 和 Mg 元素的固溶强化效果减弱,焊缝硬度和强度随着激光功率的增加而降低。激光功率为 3.6 kW 时,焊接接头获得最佳的力学性能,焊缝平均硬度和抗拉强度分别达到基材的 65%(85 HV)和 64%(271 MPa)。

参 考 文 献

[1] Kaneko R S, Bakow L, Lee E W. Aluminum alloy 6013 sheet for new US Navy aircraft[J]. JOM, 1990, 42(5): 16-18.

[2] Miller W S, Zhuang L, Bottema J, et al. Recent development in aluminium alloys for the automotive industry[J]. Materials Science and Engineering: A, 2000, 280(1): 37-49.

[3] Georgantzia E, Gkantou M, Kamaris G S. Aluminium alloys as structural material: a review of research[J]. Engineering Structures, 2021, 227: 111372.

[4] Wang X F, Guo M X, Peng W F, et al. Relationship among solution heating rate, mechanical properties, microstructure and texture of Al-Mg-Si-Cu alloy[J]. Transactions of Nonferrous Metals Society of China, 2021, 31(1): 36-52.

[5] Ninive P H, Strandlie A, Gulbrandsen-Dahl S, et al. Detailed atomistic insight into the β″ phase in Al-Mg-Si alloys[J]. Acta Materialia, 2014, 69: 126-134.

[6] Yin D Y, Xiao Q, Chen Y Q, et al. Effect of natural ageing and pre-straining on the hardening behaviour and microstructural response during artificial ageing of an Al-Mg-Si-Cu alloy[J].

Materials & Design, 2016, 95: 329-339.
[7] Han X H, Yang Z B, Ma Y, et al. Comparative study of laser-arc hybrid welding for AA6082-T6 aluminum alloy with two different arc modes[J]. Metals, 2020, 10(3): 407.
[8] 李福泉, 冯时, 李明伟, 等. 6082铝合金激光填丝焊热影响区的软化现象[J]. 中国激光, 2018, 45(11): 1102007.
Li F Q, Feng S, Li M W, et al. Softening phenomenon of heat-affected zone in laser welding of 6082 Al alloys with filler wire[J]. Chinese Journal of Lasers, 2018, 45(11): 1102007.
[9] Braun R, Donne C D, Staniek G. Laser beam welding and friction stir welding of 6013-T6 aluminium alloy sheet[J]. Material-wissenschaft Und Werkstofftechnik, 2000, 31(12): 1017-1026.
[10] Braun R. Laser beam welding of Al-Mg-Si-Cu alloy 6013 sheet using silicon rich aluminium filler powders[J]. Materials Science and Technology, 2005, 21(1): 133-140.
[11] Zhang C, Li G, Gao M, et al. Microstructure and process characterization of laser-cold metal transfer hybrid welding of AA6061 aluminum alloy[J]. The International Journal of Advanced Manufacturing Technology, 2013, 68(5): 1253-1260.
[12] Casalino G, Mortello M, Leo P, et al. Study on arc and laser powers in the hybrid welding of AA5754 Al-alloy[J]. Materials & Design, 2014, 61: 191-198.
[13] Xin Z B, Yang Z B, Zhao H, et al. Comparative study on welding characteristics of laser-CMT and plasma-CMT hybrid welded AA6082-T6 aluminum alloy butt joints[J]. Materials, 2019, 12(20): 3300.
[14] Leo P, Renna G, Casalino G, et al. Effect of power distribution on the weld quality during hybrid laser welding of an Al-Mg alloy[J]. Optics & Laser Technology, 2015, 73: 118-126.
[15] Zhang C, Gao M, Zeng X Y. Influences of synergy effect between laser and arc on laser-arc hybrid welding of aluminum alloys[J]. Optics & Laser Technology, 2019, 120: 105766.
[16] Meng Y F, Gao M, Zeng X Y. Effects of arc types on the laser-arc synergic effects of hybrid welding[J]. Optics Express, 2018, 26(11): 14775-14785.
[17] 许飞, 杨璟, 巩水利, 等. 热输入对铝合金光纤激光穿透焊缝成形的影响[J]. 中国激光, 2014, 41(12): 1203001.
Xu F, Yang J, Gong S L, et al. Effect of heat input on weld appearance for fiber laser beam full penetration welding aluminum alloy[J]. Chinese Journal of Lasers, 2014, 41(12): 1203001.
[18] 刘婷, 赵艳秋, 周旭东, 等. 能量配比系数对铝合金激光-MIG复合焊接气孔的影响[J]. 中国激光, 2020, 47(11): 1102004.
Liu T, Zhao Y Q, Zhou X D, et al. Effect of energy ratio coefficient on pore during aluminum alloy laser-MIG hybrid welding [J]. Chinese Journal of Lasers, 2020, 47(11): 1102004.
[19] Kurz W, Bezençon C, Gäumann M. Columnar to equiaxed transition in solidification processing[J]. Science and Technology of Advanced Materials, 2001, 2(1): 185-191.
[20] 陈丹, 刘婷, 赵艳秋, 等. 晶粒尺寸对双激光束双侧同步焊接接头力学性能的影响[J]. 中国激光, 2021, 48(10): 1002120.
Chen D, Liu T, Zhao Y Q, et al. Effect of grain size on mechanical properties of double laser-beam bilateral synchronous welding joint[J]. Chinese Journal of Lasers, 2021, 48(10): 1002120.
[21] He S Z, Wang J, Zhang D L, et al. A first-principles study of the Cu-containing β″ precipitates in Al-Mg-Si-Cu alloy[J]. Materials, 2021, 14(24): 7879.
[22] Chen J H, Costan E, van Huis M A, et al. Atomic pillar-based nanoprecipitates strengthen AlMgSi alloys[J]. Science, 2006, 312(5772): 416-419.
[23] Matsuda K, Ikeno S, Uetani Y, et al. Metastable phases in an Al-Mg-Si alloy containing copper[J]. Metallurgical and Materials Transactions A, 2001, 32(6): 1293-1299.
[24] Ding L P, Orekhov A, Weng Y Y, et al. Study of the Q′ (Q)-phase precipitation in Al-Mg-Si-Cu alloys by quantification of atomic-resolution transmission electron microscopy images and atom probe tomography[J]. Journal of Materials Science, 2019, 54(10): 7943-7952.
[25] Sunde J K, Marioara C D, Holmestad R. The effect of low Cu additions on precipitate crystal structures in overaged Al-Mg-Si (-Cu) alloys[J]. Materials Characterization, 2020, 160: 110087.
[26] Yan S H, Xing B B, Zhou H Y, et al. Effect of filling materials on the microstructure and properties of hybrid laser welded Al-Mg-Si alloys joints[J]. Materials Characterization, 2018, 144: 205-218.
[27] Braun R. Nd:YAG laser butt welding of AA6013 using silicon and magnesium containing filler powders[J]. Materials Science and Engineering, 2006, 426(1): 250-262.
[28] 陈夏明, 王晓南, 董其鹏, 等. 焊丝Si含量对铝合金激光-CMT复合焊接头组织性能的影响[J]. 中国激光, 2021, 48(22): 2202003.
Chen X M, Wang X N, Dong Q P, et al. Effect of filling material with different Si content on microstructure and properties of laser-CMT aluminum alloy joints[J]. Chinese Journal of Lasers, 2021, 48(22): 2202003.
[29] Beiranvand Z M, Ghaini F M, Naffakh-Moosavy H, et al. Magnesium loss in Nd: YAG pulsed laser welding of aluminum alloys[J]. Metallurgical and Materials Transactions B, 2018, 49(5): 2896-2905.
[30] Zhang C, Gao M, Wang D Z, et al. Relationship between pool characteristic and weld porosity in laser arc hybrid welding of AA6082 aluminum alloy[J]. Journal of Materials Processing Technology, 2017, 240: 217-222.
[31] Ascari A, Fortunato A, Orazi L, et al. The influence of process parameters on porosity formation in hybrid LASER-GMA welding of AA6082 aluminum alloy[J]. Optics & Laser Technology, 2012, 44(5): 1485-1490.
[32] 温鹏, 栗忠秀, 张松, 等. 摆动光纤激光-CMT复合焊接6A01-T5铝合金型材接头的气孔特征及组织性能研究[J]. 中国激光, 2020, 47(8): 0802003.
Wen P, Li Z X, Zhang S, et al. Investigation on porosity, microstructures and performances of 6A01-T5 aluminum alloy joint by oscillating fiber laser-CMT hybrid welding[J]. Chinese Journal of Lasers, 2020, 47(8): 0802003.
[33] 蔡创, 谢佳, 刘致杰, 等. 铝合金摆动激光-MIG复合焊接特性及气孔控制[J]. 中国激光, 2021, 48(18): 1802002.
Cai C, Xie J, Liu Z J, et al. Welding characteristics and porosity control of weaving laser-MIG hybrid welding of aluminum alloys [J]. Chinese Journal of Lasers, 2021, 48(18): 1802002.

Effect of Laser Power on Microstructure and Properties of High Strength Al-Mg-Si-Cu Alloy Laser-CMT Hybrid Welded Joints

Zhang Luzhong[1,2], Wang Xiaonan[2*], Chen Xiaming[2,3], Chen Wengang[1**], Li Xiang[4], Nagaumi Hiromi[3]

[1]*School of Machinery and Transportation, Southwest Forestry University, Kunming* 650224, *Yunan, China*;
[2]*School of Iron and Steel, Soochow University, Suzhou* 215021, *Jiangsu, China*;
[3]*High-Performance Metal Structural Materials Research Institute, Soochow University, Suzhou* 215021, *Jiangsu, China*;
[4]*Wuxi Raycus Fiber Laser Technology Co., Ltd., Wuxi* 214174, *Jiangsu, China*

Abstract

Objectives As a heat-treatable high-strength aluminum alloy with low density, good mechanical properties, easy forming, and corrosion resistance, Al-Mg-Si alloys have been widely used in high-speed railroads, automobiles, aerospace, and other fields. The addition of Cu to Al-Mg-Si alloys is more economical and applicable. It improves the mechanical properties and age-hardening efficiency at peak aging, resulting in ultimate tensile strength of 400 MPa at peak aging for high-strength Al-Mg-Si-Cu alloys, which is significantly higher than that of existing commercial Al-Mg-Si alloys. Softening the heat-affected zone during welding is a major problem that limits the use of heat-treatable aluminum alloys. Laser-CMT composite welding (CMT, cold metal transfer) is a promising high-performance, low-welding distortion technology that utilizes the advantages of laser and CMT welding to overcome the shortcomings of both single-laser and traditional arc welding, while increasing productivity and improving welding quality. Therefore, this study investigates the effects of laser power on the macroscopic morphology and tissue properties of the welded joints of high-strength Al-Mg-Si-Cu alloys and evaluates the possibility of applying laser-CMT composite welding technology to high-strength Al-Mg-Si-Cu alloys.

Methods In this study, a high strength Al-Mg-Si-Cu alloy with a thickness of 2 mm and filler wire with a diameter of 1.2 mm were used. A 6-kW laser and arc welding machine were used for butt-welding laser-CMT hybrid welding experiments. The welding parameters were as follows: laser powers of 3.0, 3.6, 4.2, and 4.8 kW; wire-feeding speed of 4 m/min; welding speed of 4 m/min; laser beam diameter of 0.3 mm, and the distance of 3 mm between the laser beam and arc . The specimens were then etched using the Keller reagent (1 mL HF, 1.5 mL HCl, 2.5 mL HNO_3, and 95 mL H_2O). The microstructures of the fusion zone and bead dimensions for every welding condition were examined using an optical microscope (OM). The weld microstructure was analyzed using scanning electron microscopy (SEM) after polishing and without a chemical etchant. The Vickers microhardness was measured along the joint cross-section. Dogbone-shaped samples for tensile testing were cut from the weldment perpendicular to the weld fusion line. A tensile strength test of the hybrid joint was performed at room temperature on a tensile machine.

Results and Discussions The macro morphology of the welded joint (Fig. 3) indicates that a full penetration weld is obtained when the laser power is higher than 3.6 kW. Statistical analysis results of the welded joint indicates that as the laser power increases, the upper and root melting widths of the weld increase from 3.6 mm to 4.0 mm and 2.0 mm to 2.5 mm, respectively, while the reinforcement height decreases slightly (Fig. 4). The central area of the weld possesses the typical as-cast structure, containing several equiaxed grains and little porosity (Fig. 5). When the heat input increases, the cooling rate decreases, which leads to a decrease in subcooling and promotes the growth of columnar crystals. The average width of the columnar crystal band near the bond line is 134 μm, 152 μm, and 232 μm when the laser power is 3.6 kW, 4.2 kW, and 4.8 kW, respectively (Fig. 6). The microhardness distribution patterns of the three welded joints are similar, with the weld and heat affected zone (HAZ) hardnesses being significantly lower than those for the base material (~130 HV). The average hardnesses of the weld and HAZ show a decreasing trend with increasing laser power (Fig. 7). The lower weld hardness and porosity weaken the joint, which eventually leads to the fracture of the welded joint at the seam. The joint tensile strength is the highest (271 MPa) when the laser power is 3.6 kW, while the joint tensile strengths are 244 MPa and 220 MPa for laser powers of 4.2 kW and 4.8 kW, respectively. The highest weld tensile strength occurs at low laser powers, with the joint possessing the tensile strength of approximately 64% of that of the base material at the power of 3.6 kW (Fig. 8).

Conclusions Laser-CMT composite welding is developed to combine high strength Al-Mg-Si-Cu alloys. The

characteristics of the welded joint are altered by changing the laser power. Full penetration joints are obtained when the laser power is higher than 3.6 kW. The weld width increases and the reinforcement height decreases slightly with increasing laser power. The weld consists of columnar and equiaxed crystals, and the columnar zone of the weld widens with increasing laser power (from 134 μm at 3.6 kW to 232 μm at 4.8 kW). Increasing the laser power also increases the weld dilution and Mg burnout; this decreases the Si and Mg concentrations in the weld, reducing their solid solution strengthening effects. Consequently, the weld hardness and strength decrease with increasing laser power. Overall, the best mechanical properties of the welded joint are obtained at a laser power of 3.6 kW, with the average hardness and tensile strength of the weld reaching 65% (85 HV) and 64% (271 MPa), respectively, of the base material.

Key words laser technique; high strength Al-Mg-Si-Cu alloy; laser-CMT hybrid welding; microstructure; mechanical properties